Biodegradable Fumarate-Based PolyHIPEs as Tissue Engineering Scaffolds

Elizabeth M. Christenson,[†] Wafa Soofi,[†] Jennifer L. Holm,[†] Neil R. Cameron,[‡] and Antonios G. Mikos*[,†]

Department of Bioengineering, Rice University, Houston, Texas 77251-1892, and Department of Chemistry, University of Durham, Durham, United Kingdom

Received June 28, 2007; Revised Manuscript Received September 11, 2007

PolyHIPEs show great promise as tissue engineering scaffolds due to the tremendous control of pore size and interconnectivity afforded by this technique. Highly porous, fully biodegradable scaffolds were prepared by polymerization of the continuous phase of high internal phase emulsions (HIPEs) containing the macromer poly(propylene fumarate) (PPF) and the cross-linker propylene fumarate diacrylate (PFDA). Toluene was used as a diluent to reduce the viscosity of the organic phase to enable HIPE formation. A range of polyHIPE scaffolds of different pore sizes and morphologies were generated by varying the diluent concentration (40–60 wt %), cross-linker concentration (25–75 wt %), and macromer molecular weight (M_n = 800–1000 g/mol). Although some formulations resulted in macroporous monoliths (pore diameter >500 μm), the majority of the polyHIPEs studied were rigid, microporous monoliths with average pore diameters in the range 10–300 μm. Gravimetric analysis confirmed the porosity of the microporous monoliths as 80–89% with most scaffolds above 84%. These studies demonstrate that emulsion templating can be used to generate rigid, biodegradable scaffolds with highly interconnected pores suitable for tissue engineering scaffolds.

Introduction

Engineered bone grafts provide a means to regenerate bone without the complications associated with traditional transplants.[1,2] Tissue engineers utilize a biomaterial scaffold to sustain functionality during regeneration and serve as a template for the necessary cellular interactions. Scaffolds are seeded with osteoblasts or mesenchymal cells prior to implantation in order to establish new centers for bone formation. Alternatively, cells can be recruited to the site of repair after implantation from local bone marrow.[3–6] The biomaterial chosen for these scaffolds must meet certain criteria to facilitate these processes including biocompatibility, osteoconductivity, and biodegradability.[1,7,8] In addition to the choice of a suitable biomaterial, the success of tissue engineering constructs depends on the three-dimensional architecture of the scaffold. An interconnected porous structure enables cellular migration and proliferation, vascularization, and the transport of nutrients and metabolic waste.[4,6,9,10] The mechanical properties of the scaffold are especially important in orthopedic applications. Adequate support similar to the native bone is necessary to allow for continued loading and prevent stress-shielding effects.[11,12] The advancement of bone tissue engineering strategies is strongly dependent on the development of high-porosity scaffolds that meet these mechanical strength requirements.

The fabrication process dictates scaffold properties such as architecture, surface chemistry, biodegradation, and strength.[9] A number of fabrication techniques are currently under investigation to produce porous, biodegradable scaffolds for tissue engineering applications. The most common techniques include particulate leaching, gas foaming, and fiber bonding.[6,9–11,13] Particulate leaching involves the selective leaching of a porogen, usually NaCl salt, to generate a porous morphology. Particulate leaching methods provide effective control of porosity and pore size by varying the size and dimensions of the porogen particle. Scaffolds with up to 90% porosity and pore size ranging from 100 and 800 μm have been reported.[13] However, the lack of interconnectivity between the pores at low porogen content is a large drawback of this method, and the irregular shapes of salt crystals result in poor mechanical properties of the scaffold.[11] Gas foaming utilizes two types of blowing agents to generate porous polymer scaffolds. A chemical blowing agent yields gaseous decomposition products at elevated temperatures generating bubbles within the polymer. In a physical blowing agent system, a gas is dissolved at elevated pressure, which expands to form bubbles when rapidly vented. However, these foaming techniques generally lead to pore structures that are not fully interconnected and have a "skin–core" structure where the core is porous and the external skin of the sample is solid.[14] Electrospinning, one of the most common fiber bonding techniques, has been used extensively in recent years to fabricate tissue engineering scaffolds. The relatively simple and inexpensive setup of this technique consists of a syringe pump, a high voltage source, and a collector. During electrospinning, an electric field is applied to a polymer solution to induce charge repulsion within the solution. This electrostatic force opposes the surface tension holding the solution at the syringe tip and initiates a jet stream. The solvent evaporates during transport to the collector, yielding a fine fiber. The nonwoven, electrospun scaffold is a completely open porous structure with reported porosities greater than 90%. Although extremely versatile, the pore size of these scaffolds is generally limited to less than 50 μm.[15] Solid free-form fabrication techniques such as stereolithography, selective laser sintering, and fused deposition modeling are also being explored. These techniques require

* Corresponding author. Dr. Antonios G. Mikos, Department of Bioengineering - MS142, Rice University, P.O. Box 1892, Houston, TX 77251-1892, Tel: (713) 348-5355, Fax: (713) 348-4244, E-mail: mikos@rice.edu.
[†] Rice University.
[‡] University of Durham.

10.1021/bm7007235 CCC: $37.00
Published on Web 11/03/2007

extensive setup and are limited to porosities lower than 70% and pore sizes greater than 50 μm.[16]

Emulsion templating is a relatively new method for the production of highly porous scaffolds and involves the template polymerization of high internal phase emulsions (HIPEs).[17] HIPEs are characterized by a droplet phase volume fraction of at least 74%.[18] The continuous phase contains a monomer that is polymerized and locks in the emulsion geometry at the gel point. The droplet phase is then removed, and the resulting porous scaffold is known as a polyHIPE.[19] A wide range of porosities (75–99%), pore sizes (5–100 μm), and closed- or open-pore morphologies can be achieved by varying the HIPE composition.[20–34] PolyHIPEs have great potential as tissue engineering scaffolds due to this tremendous control of scaffold morphology, potential as an injectable system, and superior mechanical properties.[17,20–26] Poly(styrene–divinylbenzene) systems are the most widely studied polyHIPEs and have recently been investigated as tissue engineering scaffolds.[20–23] Akay et al. first reported the use of polyHIPEs as support structures for animal cell growth in the patent literature.[35] However, the styrene-based system is nonbiodegradable, which led to the investigation of polyHIPEs based on poly(ε-caprolactone-*co*-styrene), poly(lactic acid-*co*-styrene), dextran, pullulan, and gelatin.[17,24,26]Although highly porous polyHIPEs were prepared with these formulations, their application to bone tissue engineering strategies were restricted due to the limited biodegradability of the copolymer systems and the low mechanical strength of the natural polymers.

The goal of our research was to fabricate fully biodegradable, rigid polyHIPE scaffolds as potential bone graft materials. The choice of macromer was limited to materials with reported biocompatibility, biodegradability, osteoconductivity, and strength.[1,7] Furthermore, successful HIPE macromers must also possess reactive double bonds and have relatively low viscosity.[17,24] Poly(propylene fumarate) (PPF) is an unsaturated polyester that biodegrades via ester hydrolysis into the biocompatible compounds fumaric acid and propylene glycol.[36,37] When reacted with the cross-linker propylene fumarate diacrylate (PFDA), this system forms a highly cross-linked network that imparts mechanical strength sufficient for its use in bone tissue engineering scaffolds.[11,36–38] Previous studies with fumarate-based scaffolds have demonstrated its biocompatibility, biodegradability, and osteoconductivity.[36–40] Fumarate-based macromers were therefore concluded to be an ideal choice for polyHIPE tissue engineering scaffolds. In this study, a range of highly porous, fully biodegradable scaffolds were prepared by polymerization of the continuous phase of HIPEs containing PPF and PFDA. The effect of composition on emulsion stability and subsequent scaffold morphology is described.

Materials and Methods

Materials. All chemicals were used as received. Propylene oxide was purchased from Acros (Pittsburgh, PA). All other chemicals were purchased from Aldrich (Milwaukee, WI).

PPF Synthesis. PPF was synthesized in a two-step process as previously described.[41,42] Briefly, diethyl fumarate and propylene glycol were reacted in the presence of a $ZnCl_2$ catalyst (molar ratio 1:3:0.01, respectively) at 145 °C under a nitrogen blanket. Hydroquinone (0.001 mol) was added to inhibit cross-linking during the synthesis. Transesterification of the diester product was conducted at 120 °C under vacuum (<1 mmHg) to produce PPF. PPF was purified as described previously, and the remaining product was vacuum-dried to remove organic solvents. The molecular weight of PPF was determined relative to polystyrene standards by gel permeation chromatography (GPC) as described below. ^{1}H NMR (250 MHz, $CDCl_3$) was used to confirm the structure of the resulting polymer: δ 1.3 (m, 3H, CH_3), 4.3 (m, 2H, CH_2), 5.3 (m, 1H, CH), 6.9 (bs, 2H, $-$CH=CH–).[35,41]

PFDA Synthesis. PFDA was synthesized in a two-step reaction.[43] First, propylene oxide was added dropwise to a solution of fumaric acid and pyridine in 2-butanone (molar ratio 2.3:1:0.03, respectively). The solution was refluxed at 80 °C for 18 h to permit full reaction of the fumaric acid. Following purification, the solvent was removed by rotary evaporation to yield the diester bis(1,2 hydroxypropyl) fumarate. In the second reaction, triethylamine was added dropwise to a solution of the diester in methylene chloride under a nitrogen blanket. The reaction was maintained at low temperature to reduce undesired side reactions utilizing a salt/ice bath. Acryloyl chloride was slowly added dropwise such that the reaction temperature did not exceed -10 °C. The molar ratio of diester, acryloyl chloride, and triethylamine was 1:2.5:2.1, respectively. After the addition of acryloyl chloride, the reaction was stirred overnight. The triethylamine salt was filtered off, and the solution was washed with 0.2 M NaOH/brine solution (6:4, v/v) until basic to remove acidic byproducts. The solution was then washed twice with brine to remove residual water, and the methylene chloride was removed by rotary evaporation. The product was then dissolved in 300 mL diethyl ether and filtered to remove high molecular weight, cross-linked species. The solution was further purified with activated charcoal to remove amine byproducts and dried with anhydrous sodium sulfate. Organic solvents were removed by rotary evaporation and dried under vacuum. ^{1}H NMR (250 MHz, $CDCl_3$): δ 1.3 (m, 3H, CH_3), 4.2 (m, 2H, CH_2), 5.2 (m, 1H, CH), 5.8 (m, 1H, –CH=CH_2), 6.1 (m, 1H, =CH–CH_2), 6.4 (dd, 1H, –CH=CH_2), 6.8 (bs, –CH=CH–).[36]

Gel Permeation Chromatography. Molecular weight distributions of PPF were determined by GPC.[42] The GPC system used consisted of an HPLC pump (Waters, model 510, Milford, MA), an autosampler (Waters, model 717), a chromatography column (Waters, Styragel HR 4E, 7.8 × 300 mm column [50–100 000 Da range]), and a differential refractometer (Waters, model 410). Degassed chloroform was used as the eluent, and a flow rate of 1.0 mL/min was used for sample measurement. A calibration curve based on polystyrene standards was used to calculate molecular weight distributions. Each sample was run in quadruplet, and the mean values for number average molecular weight (M_n) and polydispersity index (PI) were reported.

HIPE Preparation. PPF and PFDA were mixed with toluene and the surfactant sorbitan monooleate (20 wt % Span 80) prior to emulsification (Table 1). This mixture was then added to a three-neck round-bottom flask and stirred with a glass stirring rod fitted with a D-shaped PTFE paddle connected to an overhead stirrer motor. The aqueous solution, comprising potassium persulfate (2 wt % based on organic phase) and calcium chloride (1% v/v) in deionized water, was added dropwise at a rate of 1 mL/min using a peristaltic pump while constant stirring at 300 rpm was maintained. Concentrations of macromer and aqueous phases were adjusted to yield 90:10 polyHIPE foams. Constant stirring was maintained while the aqueous phase was added and the HIPE formed. Once all the aqueous phase had been added, stirring was continued for an additional 60 s to improve emulsion uniformity. The HIPE was then transferred to a 50 mL polypropylene tube and immersed in a water bath at 60 °C for 48 h. Cross-linking of the macromer chains during cure locked in the emulsion geometry of the HIPE. The bulk of the liquid was then removed in an oven at 60 °C for 12 h, and drying was completed in vacuo at room temperature for 2 h.

Previously, Timmer et al. characterized the network structure formed by the reaction of PPF and PFDA by analyzing the extractables after accelerated degradation.[43] Accelerated degradation testing was used to isolate the unreacted species by analyzing the corresponding unsaturated organic acids that were released from the network. Quantification of these components provided an estimate of the double bond conversion of the fumarate and acrylate functional groups. As expected, the acrylate double bond conversion was significantly high

Table 1. PolyHIPE Formulations

PPF M_n	PPF/PFDA ratio	toluene concentration	viscosity[a] (cSt)	porosity[b] (%)	average pore diameter[c] (μm)	average interconnect diameter[c] (μm)
800	3:1	40%	11.03 ± 0.03	84 ± 3	340 ± 91	closed pore
	3:1	50%	5.35 ± 0.03	85 ± 1	336 ± 100	closed pore
	3:1	60%	2.97 ± 0.03	macroporous	NA[d]	NA
	1:1	40%	8.38 ± 0.06	89 ± 1	49 ± 40	3 ± 1
	1:1	50%	4.36 ± 0.01	87 ± 1	35 ± 27	5 ± 2
	1:1	60%	2.58 ± 0.01	80 ± 1	58 ± 32	closed pore
	1:3	40%	6.23 ± 0.03	89 ± 1	14 ± 10	2 ± 1
	1:3	50%	3.57 ± 0.01	88 ± 1	11 ± 6	3 ± 1
	1:3	60%	2.24 ± 0.01	85 ± 2	79 ± 32	closed pore
1000	3:1	40%	18.34 ± 0.02	macroporous	NA	NA
	3:1	50%	8.57 ± 0.06	macroporous	NA	NA
	3:1	60%	4.24 ± 0.01	extensive phase separation	NA	NA
	1:1	40%	12.01 ± 0.03	85 ± 1	352 ± 45	closed pore
	1:1	50%	5.65 ± 0.02	85 ± 1	333 ± 197	closed pore
	1:1	60%	3.34 ± 0.10	macroporous	NA	NA
	1:3	40%	6.73 ± 0.01	88 ± 2	20 ± 9	3 ± 2
	1:3	50%	3.46 ± 0.05	88 ± 1	15 ± 9	3 ± 1
	1:3	60%	2.31 ± 0.01	82 ± 5	63 ± 27	closed pore

[a] Kinematic viscosity, sample size (N) = 4, average ± standard deviation. [b] Gravimetric porosity, N = 18, average ± standard deviation. [c] Average pore and interconnect measurements from image analysis of scanning electron micrographs, N = 75, average ± standard deviation. [d] NA = samples were not analyzed by SEM due to macroporous morphology or extensive phase separation.

than the fumarate double bond conversion; however, a significant fraction of the fumarate groups did react during the initial cure period and continued to cross-link over time.

SEM Analysis. Scanning electron microscopy (SEM) was used to characterize the resulting monoliths and correlate experimental parameters with scaffold morphology. All microporous specimens were vacuum-dried for an additional 12 h prior to imaging. Fractured specimens were mounted on aluminum stages, sputter-coated with gold, and examined with an FEI-XL 30 environmental scanning electron microscope. Characteristic micrographs were recorded at magnifications of 100×, 250×, and 1000×. Micrographs taken at 1000× were used for the evaluation of the average pore and interconnect size when the pore size was below 25 μm, micrographs at 250× were used for pores 25–100 μm, and micrographs at 100× were used for pores greater than 100 μm. Interconnect sizes were measured using micrographs at 1000×. Theses magnifications were chosen to provide a large sampling area for each pore range. Measurements were made on the first 25 pores and 25 interconnects from the top of the image using the image analysis software *Image J* (NIH Image).[45] Pore and interconnect measurements were made on three characteristic polyHIPE specimens for each formulation for a total of 75 measurements. However, the values measured were an underestimate of the equatorial values of the void diameters. A statistical correction was calculated by evaluating the average of the ratio R/r from

$$h^2 = R^2 - r^2 \quad (1)$$

where R is the equatorial value of void diameter, r is the diameter value measured from the micrograph, and h is the distance from the center. The probability that the sectioning takes place at any distance from the center is the same for all values of h, so the average probability value of h is $R/2$. Replacing this value in eq 1 gives $R/r = 2/(3^{1/2})$.[44,45] The average values measured from the micrographs were multiplied by this correction factor to provide a more accurate prediction of void diameter.

Viscosity Measurements. The viscosity of the organic phase of each HIPE formulation was determined using an Ubbelohde viscometer (no. 1B, Cannon Instrument Company, State College, PA) according to ASTM standard D445. The efflux time for each PPF/PFDA/toluene solution was measured in triplicate at 23 °C. Kinematic viscosities were then calculated by multiplying the efflux time in seconds by the viscometer constant, 0.05531 cSt/s. The reported values are the average kinematic viscosities and the associated standard deviations.

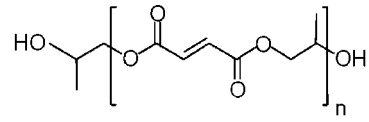

Poly(Propylene Fumarate) (PPF)

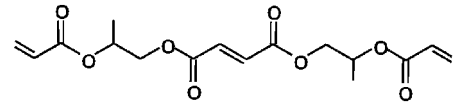

Propylene Fumarate Diacrylate (PFDA)

Figure 1. Structure of poly(propylene fumarate) (PPF) and propylene fumarate diacrylate (PFDA).

Statistical Analysis. The data are expressed as mean ± standard deviation for each treatment group. A single factor analysis of variance (ANOVA) was performed to determine whether statistical differences existed between the pore diameters measured in each polyHIPE composition. All tests were carried out with a 95% confidence intervals ($P < 0.05$).

Results and Discussion

Synthesis of PPF and PFDA. The structures of the fumarate-based polymers, PPF and PFDA, synthesized in these studies are shown in Figure 1. PPF was synthesized by a two-step procedure developed in our laboratory.[41,42] A diester intermediate, di-(2-hydroxypropyl) fumarate, was synthesized, and molecular weight increased upon transesterification of the diester.

PPF molecular weight was controlled by varying the transesterifcation time while monitoring with GPC.[41] In this study, two batches of PPF were synthesized: PPF 1000 (M_n = 960 ± 30, PI = 1.85 ± 0.12) and PPF 800 (M_n = 820 ± 10, PI = 1.71 ± 0.09) (Figure 2). The synthesized structure of PPF was confirmed with ^{1}H NMR as previously described (Figure 3).[36,42]

The cross-linker, PFDA, was synthesized by the reaction of the di-(2-hydroxypropyl) fumarate with acryloyl chloride. Although both PPF and PFDA go through the same diesCDV

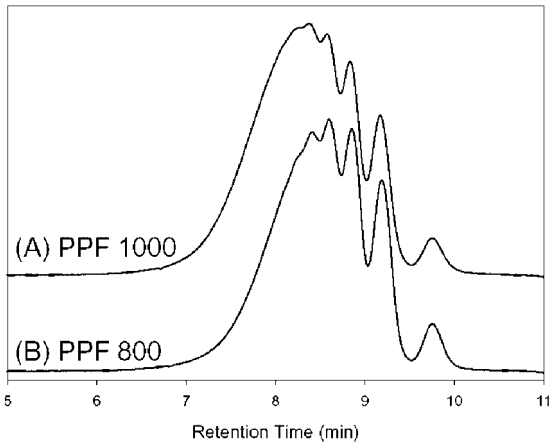

Figure 2. Gel permeation chromatograms of poly(propylene fumarate) (PPF).

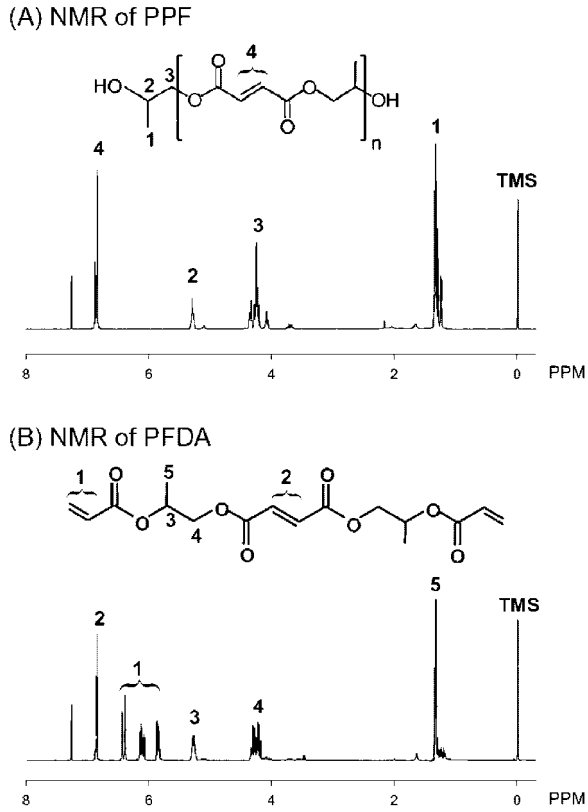

Figure 3. Nuclear magnetic resonance spectra of poly(propylene fumarate) (PPF) and propylene fumarate diacrylate (PFDA).

intermediate, two separate synthesis routes were used. The reaction of diethyl fumarate and propylene glycol used in the PPF synthesis procedure resulted in dimers and trimers, as well as the individual diester unit. Whereas the synthesis route used for PFDA resulted in a relatively monodisperse product as confirmed by GPC and ^{1}H NMR. The integration ratio of acryl protons to fumarate protons in the ^{1}H NMR spectra (Figure 3) confirmed the structure of PFDA as a single fumarate unit with two terminal acrylate groups, as previously described.[36] This ratio indicated that both terminal hydroxyl groups in the diester intermediate were acrylated.

PolyHIPE Fabrication. Toluene was used as a diluent to reduce the viscosity of the organic phase to enable HIPE formation.[34] The concentrations of PFDA (25–75%) and two PPF molecular weights, PPF 800 and PPF 1000, were also varied to examine the effect of composition on scaffold morphology. All formulations presented here formed a viscous, opaque white emulsion upon full incorporation of the aqueous phase. After cross-linking in a 60 °C water bath for 48 h, three distinct polyHIPE morphologies were observed. Images of these morphologies are given in Figure 4 and the morphology of each formulation is reported in Table 1. One of the HIPEs exhibited rapid phase separation as indicated by a dramatic loss of volume of the resulting cross-linked polymer (Figure 4A). Several of the polyHIPEs were visibly macroporous with pore diameters on the order of millimeters as measured by light microscopy (Figure 4B). The remaining polyHIPEs were rigid, microporous monoliths (Figure 4C,D). The compressive modulus of the microporous monoliths was on the order of 1–5 MPa. Less than 5% shrinkage of the overall volume of the microporous polyHIPEs was observed. Gravimetric analysis of the porosity also indicated that all microporous polyHIPEs retained 80–89% porosity with most scaffolds above 84% (Table 1). It is noteworthy that the definitions of macroporosity and microporosity used here differ from the IUPAC definitions used for catalysis applications (microporous <2 nm pore diameter; macroporous >40 nm pore diameter). However, the definitions used in this manuscript are consistent with the established tissue engineering nomenclature (microporous 10–500 μm; macroporous >500 μm).[9,44]

SEM analysis was used to characterize the open- and closed-pore microstructures of the microporous polyHIPEs. Closed-pore morphologies (Figure 4C) were characterized by discrete pores without windows to other pores. A thin film was apparent between the pores in SEM. Tearing of this film was occasionally observed and was attributed to rupture during drying of the scaffolds. In contrast, the polyHIPEs with open-pore morphology (Figure 4D) had several windows that connected to other pores. Cameron et al. reported cryo-SEM experiments that correlated the formation of these windows or interconnects with the polymerization gel point.[46] The interconnect formation was attributed to the shrinkage of the thin polymer film separating droplets that occurs due to the conversion of monomer to higher-density polymer. If the film was sufficiently thin, this shrinkage would result in a window opening and expanding. Therefore, the presence and size of interconnects are dependent on the film thickness, which is in turn dependent on droplet size and interfacial tension.

It was observed that polyHIPEs with pores greater than 50 μm had a closed-pore morphology, whereas scaffolds with pores smaller than 50 μm had an open-pore morphology (Figure 5). The two morphologies were attributed to differences in film thickness between the droplets at the gel point. It was hypothesized that the film thickness of the closed-pore polyHIPEs was thick enough to withstand the thinning of the film during polymerization without interconnect formation. The open-pore polyHIPEs were therefore concluded to have films sufficiently thin to allow for interconnect formation. Given that the volume is constant, a smaller droplet size would result in a larger surface area. Conservation of the organic phase indicates that an increase in surface area would result in a reduction in the amount of continuous phase around each droplet. Therefore, it was concluded that the smaller droplet size resulted in a reduction of film thickness below the threshold value that permits interconnect formation.

Akay et al. reported different pore architectures in polyHIPE scaffolds.[35] Basic or primary pores were described as the initial pores formed during the emulsification stage and were characterized by large interconnect sizes relative to the

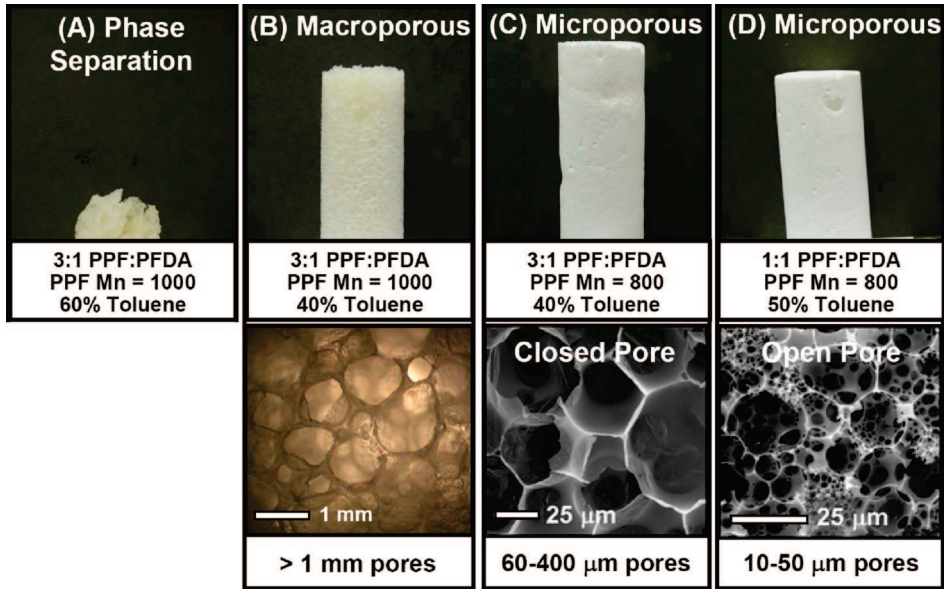

Figure 4. Fumarate-based polyHIPE morphologies. PolyHIPEs are cylinders ~25 mm in diameter.

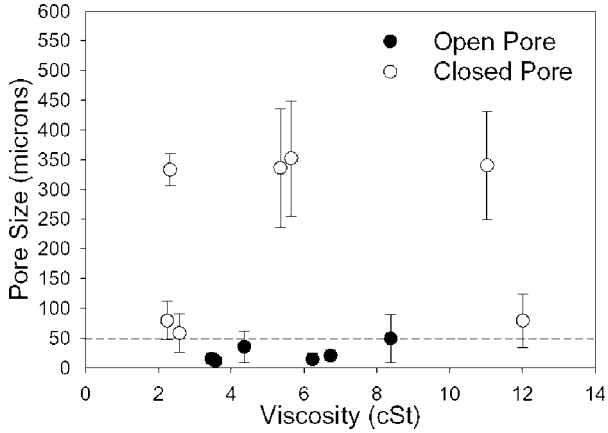

Figure 5. Plot of the kinematic viscosity of the organic phase vs the average pore size of the fumarate-based polyHIPEs. Pore sizes are reported as average ± standard deviation, $N = 75$.

pore size (Figure 4D), whereas coalescence pores were obtained through the coalescence of primary pores during polymerization. Pore sizes of the latter are generally much larger than primary pores and can exceed 5 mm. These pores are often closed or have much smaller interconnect sizes. Coalescence pores were observed to some extent in most of the systems studied. The size and frequency of coalescence pores were inversely related to the stability of the system. In general, the open-pore polyHIPEs had few coalescence pores, and the pores were generally on the same order of size as the primary pores.

Effect of Diluent Concentration. In addition to reducing the viscosity of the continuous phase to permit the formation of the HIPE, diluents can also affect the stability of the emulsion. Once formed, HIPEs are only stable kinetically, and the rate of droplet coalescence and phase separation is a measure of the emulsion stability. Emulsion stability is dependent on the (1) interfacial tension between the two phases; (2) viscosity of the continuous phase; (3) volume fraction of the dispersed phase; and (4) temperature during formation and cure of the HIPE.[24,47] These factors must be addressed in the design of any HIPE system. A sufficiently low viscosity is required to permit efficient mixing of the phases and dispersion of the droplet phase. However, a lower viscosity also corresponds to increased mobility of the continuous phase that can accelerate phase separation. Increased viscosity can stabilize the emulsion by providing a kinetic barrier to droplet coalescence. One can conclude that the optimal polyHIPE design would be a continuous phase with the highest viscosity that permits efficient mixing of the two phases.

In this study, toluene concentrations from 30% to 70% of the organic phase were studied to determine the effect of viscosity on polyHIPE morphology. Only formulations from 40% to 60% toluene formed stable HIPEs reproducibly. It was hypothesized that the viscosity of the organic phase at less than 40% toluene was too high to permit formation of the emulsion, whereas the viscosity at more than 60% toluene resulted in unstable emulsions with very rapid rates of phase separation. The viscosity of the organic phases (PPF, PFDA, toluene) of all compositions are reported in Table 1. Increasing the toluene concentration from 40% to 60% resulted in a greater than 2-fold decrease in viscosity of the organic phase.

The effect of toluene concentration on the macroscopic morphology is shown in Figure 6 and summarized in Table 1. Overall, the 40 and 50 wt % toluene systems had similar morphologies, whereas the 60 wt % toluene system was less stable. For example, the 40 and 50 wt % toluene systems in Figure 6A were microporous monoliths, and the 60 wt % toluene system was a macroporous monolith. Similarly, in the compositions where the 40 and 50 wt % toluene systems were macroporous monoliths, the 60 wt % toluene system underwent extensive phase separation (Figure 6B).

SEM analysis of the microporous monoliths was conducted to determine the effect of toluene concentration on pore morphology. Pore and interconnect size in characteristic micrographs was quantified using *Image J* software (Table 1). To determine whether absolute viscosity could be used to predict emulsion stability and, thus, polyHIPE morphology, viscosity of the organic phase versus pore size was plotted (Figure 5). No direct trend regarding absolute viscosity and pore size was observed. Although no significant difference in morphology or pore size was observed between 40 and 50 wt % toluene systems, the 60 wt % toluene specimens CDV

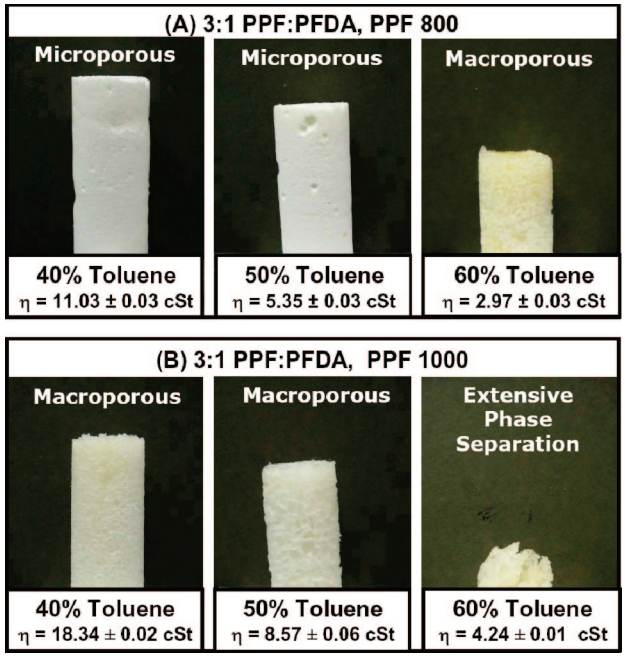

Figure 6. Optical micrographs of polyHIPEs fabricated with 40, 50, and 60 wt % diluent concentrations: (A) 3:1 PPF/PFDA, PPF 800; (B) 3:1 PPF/PFDA, PPF 1000. PolyHIPEs are cylinders ~25 mm in diameter.

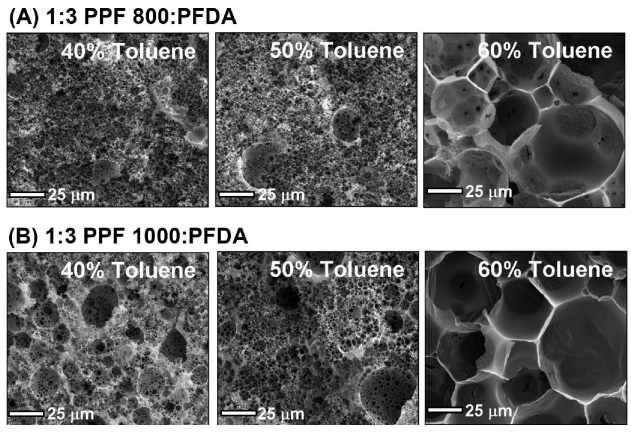

Figure 7. Scanning electron micrographs of fracture planes of polyHIPEs fabricated with 40, 50, and 60 wt % diluent concentrations: (A) 1:3 PPF/PFDA, PPF 800; (B) 1:3 PPF/PFDA, PPF 1000. Bar = 25 μm.

every composition were the least stable. Furthermore, none of the 60 wt % toluene polyHIPEs had open-pore structures (Figure 7).

Both the macroscopic morphology and the microstructure results indicate that the lower viscosity of the 60 wt % toluene systems did have an impact on polyHIPE architecture. It was hypothesized that, in an otherwise stable fumarate-based system, a viscosity below 3.5 cSt resulted in a decrease in emulsion stability. This suggests that, above this minimum viscosity, interfacial tension of the fumarate-based HIPEs was a more significant factor in determining the emulsion stability. Interfacial tension is dependent in part on the hydrophobicity of each component: PPF, PFDA, and toluene.[24]

If sufficiently different than the other components, the addition of a diluent can alter the interfacial tension between the two phases and further impact emulsion stability. The impact of toluene on the hydrophobicity of the organic phase was calculated using model predictions of the octanol–water partition

Table 2. Estimated Octanol–Water Partition Coefficients

molecule	molecular weight	log P^a
toluene	92	2.386
PFDA	340	2.296
PPF ($n = 1$)	232	0.018
PPF ($n = 2$)	388	0.625
PPF ($n = 3$)	544	1.232
PPF ($n = 4$)	700	1.839
PPF ($n = 5$)	856	2.446
PPF ($n = 6$)	1012	3.053
PPF ($n = 7$)	1168	3.660

[a] Octanol–water diffusion coefficient calculated with the Molinspiration miLogP model based on molecular structures.[48]

coefficients of PPF, PFDA, and toluene. Octanol–water partition coefficients are used in quantitative structure–property relationship (QSPR) studies as a measure of molecular hydrophobicity. It is the concentration ratio of a compound in each phase of a mixture of two immiscible solvents, typically water and a hydrophobic solvent such as octanol.[48]

$$\log P = \log\left(\frac{[\text{solute}]_{\text{oct}}}{[\text{solute}]_{\text{water}}}\right) \quad (2)$$

Thus, log P is a measure of the differential solubility of the compound between these two solvents. The method used here for log P prediction was developed at Molinspiration (miLogP2.2—November 2005).[48] Calculations of each compound were based on the sum of its nonoverlapping molecular fragments. The group contributions were obtained by fitting calculated log P with experimental log P for a training set of more than 12 000 molecules.[48] The calculated values are listed in Table 2. As expected, the hydrophobicity of PPF increased with increasing molecular weight. The log P value of toluene (2.386) was intermediate between PPF 800 (2.446) and PFDA (2.296). Therefore, the relatively small differences in hydrophobicity between toluene and PPF ($\delta = 0.06$) and between toluene and PFDA ($\delta = 0.09$) were concluded to be unlikely to impact the interfacial tension of the HIPE and the emulsion stability. The effect of PPF and PFDA on this parameter is discussed below.

Effect of Cross-linker Content. The concentration of the cross-linker can impact the emulsion stability and the resulting morphology of the polyHIPEs in a number of ways. PFDA has lower viscosity than both molecular weights of PPF studied here. Therefore, higher mass fractions of PFDA resulted in lower viscosities of the organic phase (Table 1). This reduction in viscosity could result in lower emulsion stability of the HIPE, as described in the previous section. In addition, the concentration and structure of the cross-linker can affect polyHIPE morphology by altering the cross-linking kinetics. An increase in cross-linking rate could accelerate the gelation of the HIPE and reduce the amount of droplet coalescence prior to the gel point. The rate of cross-linking is dependent on the reactivity of the double bonds, number of cross-linking sites available, and the degrees of freedom of the molecules. The acrylate groups of the PFDA molecule are more reactive than the fumarate groups, the ratio of double bonds increases with increasing PFDA concentration, and the steric hindrance associated with PFDA is less than that associated with PPF.[43] Overall, an increase in the PFDA weight fraction was assumed to increase the rate of cross-linking and therefore could accelerate gelation of the HIPE. Finally, the acrylate end-groups (Figure 1) increased the hydrophobicity of the PFDA molecule as confirmed by the increase in the log P value (Table 2). ACS

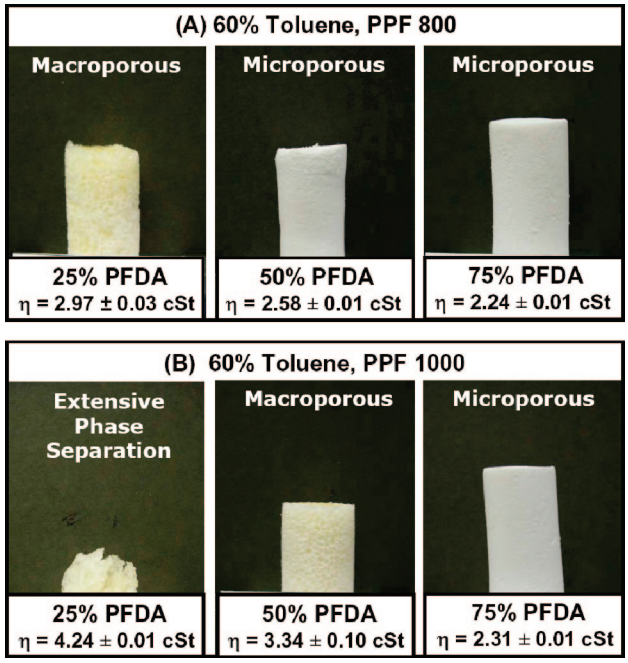

Figure 8. Optical micrographs of polyHIPEs fabricated with 25, 50, and 75 wt % cross-linker concentrations: (A) 60% toluene, PPF 800; (B) 60% toluene, PPF 1000. PolyHIPEs are cylinders ~25 mm in diameter.

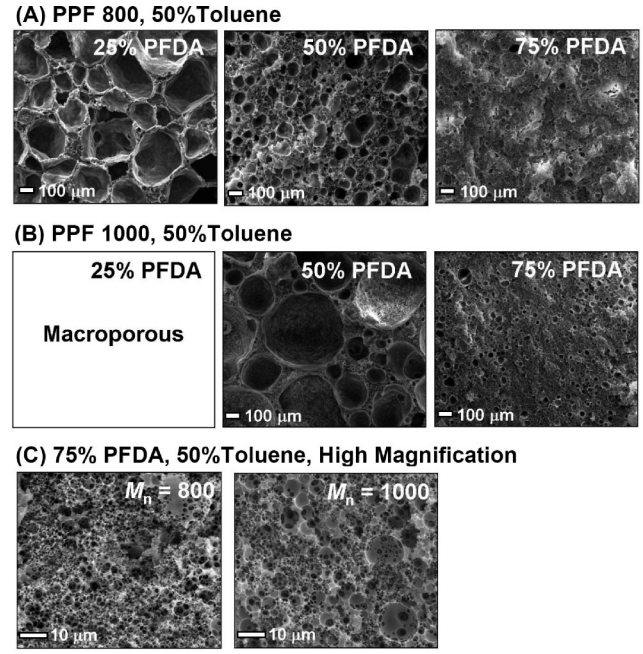

Figure 9. Scanning electron micrographs of fracture planes of polyHIPEs fabricated with 25, 50, and 75 wt % cross-linker concentrations: (A) 50% toluene, PPF 800, bar = 100 μm; (B) 50% toluene, PPF 1000, bar = 100 μm; (C) high magnification, 50% toluene, 75% PFDA, bar = 10 μm.

discussed above, this change in hydrophobicity can impact the interfacial tension and the emulsion stability.

The impact of cross-linker concentration on the macroscopic morphology of the polyHIPEs is shown in Figure 8 and summarized in Table 1. Overall, increasing the PFDA concentration resulted in a decreased amount of phase separation and droplet coalescence prior to gelation. The morphology of the PPF 800 polyHIPE in Figure 8A was macroporous at 25 wt % PFDA and microporous at both 50 and 75 wt % PFDA. Similarly, in the PPF 1000 system, extensive phase separation was observed at 25 wt % PFDA, a macroporous monolith at 50 wt % PFDA, and a microporous monolith at 75 wt % PFDA (Figure 8B).

Similar trends were observed for all HIPE compositions. Further investigation of the microstructure of the microporous polyHIPEs was conducted with SEM analysis. Figure 9A,B illustrates the effect of increasing cross-linker concentration on the pore size of the polyHIPE. Quantification of the pore sizes indicated that the average pore size decreased with increasing PFDA concentration, confirming decreased droplet coalescence prior to gelation (Table 1).

The decreased pore size with increasing PFDA concentration precludes the effect of viscosity. The reduction in viscosity would reduce the stability and result in an increase in pore size with increasing PFDA concentration. Therefore, to ascertain whether the differences in polyHIPE morphology were due to increased emulsion stability or accelerated gelation, a preliminary study on the rate of phase separation was conducted. Similar to a previous study, the HIPEs were fabricated without initiator, and the degree of phase separation was qualitatively scored over a period of 72 h.[24] The rate of phase separation decreased with increasing PFDA concentration (data not shown). This indicated that a higher PFDA concentration resulted in an increase in emulsion stability, and the differences in polyHIPE morphology were most likely not due to an increased rate of cross-linking. Therefore, it was hypothesized that the difference in the hydrophobicity of PFDA and PPF was responsible for the increased emulsion stability (Table 2). Indeed, the difference between PPF and PFDA was estimated to be larger (PPF 800, $\delta = 0.15$) than the respective differences between toluene and PPF or PFDA.

Effect of PPF Molecular Weight. PPF molecular weight can also affect HIPE stability by changing the viscosity of the organic phase and altering the interfacial tension of the system. Every HIPE system with PPF 1000 had a higher viscosity than the complementary PPF 800 composition (Table 1). This increase in viscosity could increase the stability of the emulsion, as described above. However, the results from the diluent study suggest that this relatively modest increase in viscosity (5–40%) would have little impact on the emulsion stability. Increasing PPF molecular weight also increases the hydrophobicity of the PPF molecule (Table 2). The ranking of the relative hydrophobicity based on the calculated log *P* values is PPF 700 < PFDA < toluene < PPF 800 < PPF 1000 < PPF 1200. These differences in hydrophobicity could have corresponding effects on the interfacial tension and emulsion stability of the HIPEs.

PPF with number average molecular weights (M_n) from 700 to 1200 g/mol were examined; however, only PPF with M_n of 800 and 1000 g/mol formed stable HIPEs. It was hypothesized that the viscosity at higher molecular weights inhibited efficient mixing of the phases and full incorporation of the aqueous droplet phase. The greater hydrophobicity of the PPF 1200 (Table 2) may also have affected the surface tension between the two phases and reduced emulsion stability. In contrast, it was hypothesized that the increased hydrophilicity of the lower molecular weight PPF destabilized the HIPE and resulted in rapid phase separation.

The macroscopic morphology of the PPF 800 and PPF 1000 polyHIPEs are compared in Figures 6 and 8 and summarized in Table 1. It was observed that at low concentrations of PFDA, PPF 1000 HIPEs were markedly less stable than PPF 800 HIPEs. At 25 wt % PFDA, all PPF 1000 HIPEs underwent extensive phase separation or produced macroporous polyHIPEs. How

ever, all 75 wt % PFDA HIPEs formed microporous monoliths regardless of molecular weight. SEM analysis of the polyHIPE microstructure confirmed these trends. At 25% PFDA, the PPF 800 polyHIPE was a closed-pore, microporous monolith (Figure 9A), whereas the PPF 1000 polyHIPE was a macroporous monolith (Figure 9B). In contrast, very little difference in pore size or morphology was evident at 75% PFDA (Figure 9C).

It was hypothesized that the interfacial tension of the emulsion was dependent on the relative concentration and hydrophobicity of the components of the organic phase. The log *P* value for PPF 800 (~2.446) was closer to that of PFDA (~2.296) than that of PPF 1000 (~3.053). An increase in PFDA concentration resulted in more stable emulsions. Excluding the effects of viscosity and cross-linking rate for reasons stated above, one may conclude that PFDA reduces the interfacial tension between the two phases and stabilizes the emulsion. Therefore, the increased hydrophobicity of the PPF 1000 molecule relative to PFDA would destabilize the emulsion. However, at high concentrations of PFDA, the difference in PPF molecular weight was assumed to be less significant due to the reduced presence of PPF molecules at the interface. The morphologies of the 75 wt % PFDA polyHIPEs were concluded to be the result of the interfacial tension dominated by the PFDA molecules.

Conclusions

These studies indicate that emulsion templating can be used to generate rigid, biodegradable scaffolds with interconnected pores. A range of polyHIPE scaffolds of different pore sizes and morphologies were generated by varying the diluent concentration, cross-linker concentration, and macromer molecular weight. PolyHIPEs with pores greater than 50 μm had a closed-pore morphology, whereas scaffolds with pores smaller than 50 μm had an open-pore morphology. These two morphologies were attributed to differences in film thickness between the droplets at the gel point. It was hypothesized that the films between droplets of the closed-pore polyHIPEs were thick enough to withstand the thinning of the film during polymerization without interconnect formation; whereas the open-pore polyHIPEs had films sufficiently thin to allow for interconnect formation. It was concluded that the smaller droplet size resulted in a reduction of film thickness below the threshold value that results in interconnect formation.

The effects of compositional variables on viscosity and interfacial tension were explored. It was proposed that, above a minimum viscosity, interfacial tension of the fumarate-based HIPEs was a more accurate predictor of emulsion stability and polyHIPE morphology than viscosity. Model predictions of the octanol–water partition coefficient were used to compare the relative hydrophobicity of the organic components and the impact of these differences on interfacial tension. On the basis of the experimental findings and similarity in log *P* values, it was concluded that toluene concentration had little impact on the interfacial tension. In contrast, there was a notable difference in polyHIPE morphology with increasing cross-linker concentration. An emulsion stability study confirmed that the resulting morphology was due to an increase in stability rather than accelerated cross-linking. It was therefore assumed that this effect was due to a reduction in interfacial tension at higher PFDA concentrations. This assumption was supported by the reduced stability of the HIPEs with higher molecular weight PPF. The increased hydrophobicity of the PPF 1000 molecule relative to PFDA was hypothesized to destabilize the emulsion. However, this destabilization was overcome at high concentrations of PFDA where the presence of PPF molecules at the interface was reduced. Overall, polyHIPEs show great promise as tissue engineering scaffolds due to the tremendous control of pore size and interconnectivity afforded by this technique. Further investigation of degradation profiles, mechanical properties, and cellular behavior on these scaffolds is currently in progress.

Acknowledgment. The authors acknowledge the technical assistance provided by Dr. Maria Bokhari and Dr. Ross Carnachan. Dr. Istvan Lengyel, Dr. Paul Engel, and Dr. Chris Christenson are gratefully acknowledged for invaluable technical discussions. Financial support of this research was provided by the National Institute of Dental and Craniofacial Research (1 T32 DE 015355-01, EMC and R01 DE15164, AGM). The Texas/U.K. Collaborative Research Initiative is acknowledged for travel support.

References and Notes

(1) Rose, F.; Oreffo, R. *Biochem. Biophys. Res. Commun.* **2002**, *292*, 1.
(2) Kenley, R. A.; Yim, K.; Abrams, J.; Ron, E.; Turek, T.; Marden, L. J.; Hollinger, J. O. *Pharm. Res.* **1993**, *10*, 1393.
(3) Langer, R.; Vacanti, J. P. *Science* **1993**, *260*, 920.
(4) Bhatia, S. N.; Chen, C. S. *Biomed. Microdevices* **1999**, *2*, 131.
(5) Crane, G. M.; Ishaug, S. L.; Mikos, A. G. *Nat. Med.* **1994**, *1*, 1322.
(6) Freyman, T. M.; Yannas, I. V.; Gibson, L. J. *Prog. Mater. Sci.* **2001**, *46*, 273.
(7) Seal, B. L.; Otero, T. C.; Panitch, A. *Mater. Sci. Eng.* **2001**, *R 34*, 147.
(8) Temenoff, J. S.; Mikos, A. G. *Biomaterials* **2000**, *21*, 2405.
(9) Hacker, M.; Ringhofer, M.; Appel, B.; Neubauer, M.; Vogel, T.; Young, S.; Mikos, A. G.; Blunk, T.; Gopferich, A.; Schulz, M. B. *Biomaterials* **2007**, *28*, 3497.
(10) Mikos, A. G.; Temmenoff J. S. *Electron. J. Biotechnol.* **2000**, *3* (2).
(11) Shi, X.; Sitharaman, B.; Pham, Q. P.; Liang, F.; Wu, K.; Billups, W. E.; Wilson, L. J.; Mikos, A. G. *Biomaterials* **2007**,in press.
(12) Horch, R. A.; Shahid, N; Mistry, A. S.; Timmer, M. D.; Mikos, A. G.; Barron, A. R. *Biomacromolecules* **2004**, *5*, 1990.
(13) Karageorgiou, V.; Kaplan, D. *Biomaterials* **2005**, *26*, 5474.
(14) Leatrese, D. H.; Byung-Soo, K.; Mooney, D. J. *J. Biomed. Mater. Res.* **1998**, *42*, 396.
(15) Pham, Q. P.; Sharma, U.; Mikos, A. G. *Tissue Eng.* **2006**, *12*, 1197.
(16) Cooke, M. N.; Fisher, J. P.; Dean, D.; Rimnac, C.; Mikos, A. G. *J. Biomed. Mater. Res., Part B: Appl. Biomater.* **2002**, *64B*, 65.
(17) Busby, W.; Cameron, N. R.; Jahoda, C. *Polym. Int.* **2002**, *51*, 871.
(18) Lissant, K. J., Ed. *Emulsions and Emulsion Technology Part 1*; Marcel Dekker Inc.: New York, 1974.
(19) Hainey, P.; Huxham, I. M.; Rowatt, B.; Sherrington, D. C. *Macromolecules* **1991**, *24*, 117.
(20) Akay, G.; Birch, M. A.; Bokhari, M. A. *Biomaterials* **2004**, *25*, 3991.
(21) Bokhari, M.; Birch, M.; Akay, G. *Experimental Medical Biology: Tissue Engineering, Stem Cells, and Gene Therapies* **2003**, *534*, 247.
(22) Hayman, M. W.; Smith, K. H.; Cameron, N. R.; Przyborski, S. A. *Biochem. Biophys. Res. Commun.* **2004**, *314*, 483.
(23) Hayman, M. W.; Smith, K. H.; Cameron, N. R.; Przyborski, S. A. *J. Biochem. Biophys. Methods* **2005**, *62*, 231.
(24) Busby, W.; Cameron, N. R.; Jahoda, C. *Biomacromolecules* **2001**, *2*, 154.
(25) Barbetta, A.; Dentini, M.; Zannoni, E. M.; De Stefano, M. E. *Langmuir* **2005**, *21*, 12333.
(26) Barbetta, A.; Dentini, M.; De Vecchis, M. S.; Filippini, P.; Formisano, G.; Chiazza, S. *Adv. Funct. Mater.* **2005**, *15*, 118.
(27) Barby, D.; Haq, Z. U.S. Patent 4,522,953, 1985.
(28) Cameron, N. R.; Sherrington, D. C.; Albiston, L.; Gregory, D. P. *Colloid Polym. Sci.* **1996**, *274*, 592.
(29) Cameron, N. R.; Sherrington, D. C.; Ando, I.; Kurosu, H. *J. Mater. Chem.* **1996**, *6*, 719.
(30) Williams, J. M.; Wrobleski, D. A. *Langmuir* **1988**, *4*, 656.
(31) Williams, J. M.; Gray, A. J.; Wilkerson, M. H. *Langmuir* **1990**, *6*, 437.
(32) Cameron, N. R.; Sherrington, D. C. *Macromolecules* **1997**, *30*, 5860.
(33) Barbetta, A.; Cameron, N. R.; Cooper, S. *J. Chem. Commun.* **2000**, 221.
(34) Cameron, N. R.; Barbetta, A. *J. Mater. Chem.* **2000**, *10*, 2466.
(35) Akay, G.; Downes, S.; Price, V. J. WO 00/34454, 2000.

CDV

(36) He, S.; Timmer, M. D.; Yaszemski, M. J.; Yasko, A. W.; Engel, P. S.; Mikos, A. G. *Polymer* **2001**, *42*, 1251.
(37) Shi X.; Mikos, A. G. In *An Introduction to Biomaterials,* Guelcher, S. A.; Beckman, E. J.; Hollinger, J. O., Eds.; CRC Press: Boca Raton, 2006; pp. 205–218.
(38) Timmer, M. D.; Shin, H.; Horch, R. A.; Ambrose, C. G.; Mikos, A. G. *Biomacromolecules* **2003**, *4*, 1026.
(39) Temenoff, J. S.; Mikos, A. G. *Biomaterials* **2000**, *21*, 2405.
(40) Fisher, J. P.; Vehof, J.W.M.; Dean, D.; van der Waerden, J.P.C.M.; Holland, T. A.; Mikos, A. G.; Jansen, J. A. *J. Biomed. Mater. Res.* **2002**, *59*, 547.
(41) Peter, S. J.; Suggs, L. J.; Yaszemski, M. J.; Engel, P. S.; Mikos, A. G. *J. Biomater. Sci. Polym. Educ.* **1999**, *10*, 363.
(42) Shung, A. K.; Timmer, M. D.; Jo, S.; Engel, P. S.; Mikos, A. G. *J. Biomater. Sci. Polym. Educ.* **2002**, *13*, 95.
(43) Timmer, M. D.; Horch, R. A.; Ambrose, C. G.; Mikos, A. G. *J. Biomater. Sci. Polym. Educ.* **2003**, *14*, 369.
(44) Barbetta, A.; Cameron, N. R *Macromolecules* **2004**, *37*, 3188.
(45) Carnachan, R. J.; Bokhari, M.; Przyborskib, S. A.; Cameron, N. R. *Soft Matter* **2006**, *2*, 608.
(46) Cameron, N. R.; Sherrington, D. C.; Albiston, L.; Gregory, D. P. *Colloid Polym. Sci.* **1996**, *274*, 592.
(47) Butler, R.; Hopkinson, I.; Cooper, A. I. *J. Am. Chem. Soc.* **2003**, *125*, 14473.
(48) http://www.molinspiration.com/

BM7007235